Self-Induced Dirac Boundary State and Digitization in a Nonlinear Resonator Chain

Gengming Liu,[1] Jiho Noh,[2] Jianing Zhao,[2] and Gaurav Bahl[2,*]
[1]Department of Physics, University of Illinois at Urbana-Champaign, Urbana, Illinois 61801, USA
[2]Department of Mechanical Science and Engineering, University of Illinois at Urbana-Champaign, Urbana, Illinois 61801, USA

(Received 11 April 2022; accepted 26 August 2022; published 23 September 2022)

The low-energy excitations in many condensed matter and metamaterial systems can be well described by the Dirac equation. The mass term associated with these collective excitations, also known as the Dirac mass, can take any value and is directly responsible for determining whether the resultant band structure exhibits a band gap or a Dirac point with linear dispersion. Manipulation of this Dirac mass has inspired new methods of band structure engineering and electron confinement. Notably, it has been shown that a massless state necessarily localizes at any domain wall that divides regions with Dirac masses of different signs. These localized states are known as Jackiw-Rebbi-type Dirac boundary modes and their tunability and localization features have valuable technological potential. In this study, we experimentally demonstrate that nonlinearity within a 1D Dirac material can result in a self-induced domain boundary for the Dirac mass. Our experiments are performed in a dimerized magnetomechanical metamaterial that allows complete control of both the magnitude and sign of the local material nonlinearity, as well as the sign of the Dirac mass. We find that the massless bound state that emerges at the self-induced domain boundary acts similarly to a dopant site within an insulator, causing the material to exhibit a dramatic binary switch in its conductivity when driven above an excitation threshold.

DOI: 10.1103/PhysRevLett.129.135501

The Dirac equation and its analogs are frequently encountered in a wide range of condensed matter and metamaterial systems [1–12]. A prominent characteristic of these systems is the linear dispersion relation near crossing points between their bulk bands, commonly known as Dirac points, where the collective excitations appear massless [13,14]. The degeneracy at any Dirac point is held by material-specific symmetries which, when broken, can split into a pair of states with Dirac masses of opposite signs [14]. Such regions of opposite Dirac mass have been observed in graphene [15–17], topological insulators [18–21], and various metamaterial systems such as phononic [22–24] and photonic crystals [25–27].

Notably, it has been shown that there necessarily exists a localized state on any boundary between regions with opposite Dirac masses, which was originally discussed in the context of quantum field theory by Jackiw and Rebbi [28] but has since been shown to occur in classical Dirac materials [29–35]. As an intuitive interpretation, the trapped state appears because an intermediate massless (and therefore gapless) transition must occur at the boundary for the Dirac mass to flip the sign, which resembles a metallic boundary between two gapped regions. The original Jackiw-Rebbi (JR) theory describes a topologically protected boundary mode at the midgap energy [28]. In contrast, generic boundary states in a Dirac material form via a similar process but are not topologically protected. We, therefore, describe these modes as being of JR type and these more generic states are expected to exhibit a variety of tunable in-gap dispersion such as flat bands and linear crossings [36]. Even so, the localization on the boundary is unchanged and the JR-type Dirac boundary mode is believed to contribute to long-range edge transport observed in a variety of Dirac materials [21,37,38].

In this work, we show that a domain boundary of Dirac mass, and hence a localized JR-type state, can be self-induced in a Dirac material with Duffing (third-order) nonlinearity. We experimentally implement this using a magnetomechanical approach that provides complete control over the sign and magnitude of the nonlinear coefficients [39]. We first confirm that a designed inversion of the Dirac mass in a linear system leads to the appearance of the JR-type state. Subsequently, we introduce the nonlinearity, and show that a self-induced Dirac mass boundary and a JR-type state can appear in a homogeneous system under strong driving conditions. Interestingly, we find that the induced JR-type state acts similarly to a dopant site in an insulator, resulting in a binary switch in the conductivity through the system.

We start with a brief description of the link between the equations of motion for a diatomic resonator array and the one-dimensional Dirac equation. Consider an infinite one-dimensional dimerized lattice of linear resonators with staggered resonance frequencies and constant nearest-neighbor coupling strength γ as shown in Fig. 1(a). We label the sublattices within the unit cell A and B,

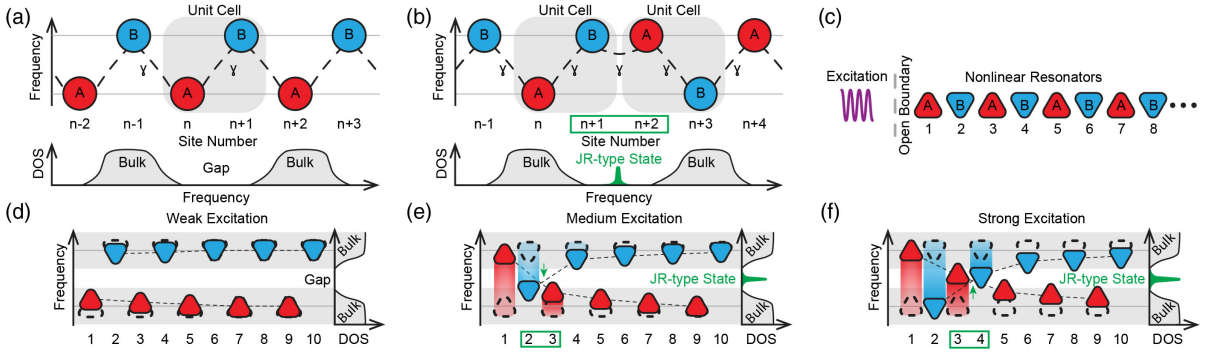

FIG. 1. Engineering Dirac boundary mode in linear and nonlinear diatomic arrays. (a) A diatomic chain with staggered resonance frequencies and uniform coupling rate (represented by curved dash lines) has a band gap (lower left) that can be shown through a measurement of the density of state (DOS). (b) A JR-type Dirac boundary state arises at the interface where the unit cell resonance frequencies are flipped. The resulting in-gap mode is shown below. (c) For nonlinear arrays, inversion of frequencies can be induced by external excitation from an edge. (d)–(f) Amplitude-dependent frequency detuning in a nonlinear chain at different excitation levels. Dash lines are used as a visual aid to locate the boundary mode.

respectively. A mismatch between the natural frequencies of the two resonators (on sublattices A and B) within a unit cell creates two-band insulators [40,41]. In between these two bands is a forbidden-frequency region (band gap) where no eigenmode exists to host excitation in the structure and thus this diatomic lattice resembles an insulator at such frequencies.

It has been shown [42,43] that the coupled-mode equations representing the discrete, classical one-dimensional lattice

$$i\frac{da_n(t)}{dt}+\gamma[a_{n+1}(t)+a_{n-1}(t)]-(-1)^n\Delta\times a_n(t)=0, \quad (1)$$

can be mapped to the 1D Dirac equation

$$i\partial_t\Psi(\xi,t)=-i\gamma\hat{\sigma}_x\partial_\xi\Psi(\xi,t)+\Delta\times\hat{\sigma}_z\Psi(\xi,t), \quad (2)$$

after a transformation to the continuous transverse coordinate. Here, a_n is the oscillation amplitude at the nth resonator, 2Δ is the resonance frequency mismatch, and $\hat{\sigma}_i$ are the Pauli matrices explicitly defined in Supplemental Material, Sec. I [44]. In this analogy, the term Δ is often called the Dirac mass. The Dirac equation famously produces solutions with positive energies as well as solutions with negative energies [45]—the latter were later proven to be antiparticles [46] labeled by the negative sign in front of their mass terms. For the rest of the Letter, we use the term "negative Dirac mass" for convenience of discussion as done in other references [1,14]. A more detailed discussion in the context of our system is also included in Supplemental Material, Sec. I [44]. Based on Eq. (1), if we define the first resonator on sublattice site A to be $n=0$, a positive Dirac mass would correspond to a chain with the A-site resonators having a higher resonance frequency than that of B-site ones. At the interface between lattices with Dirac masses of opposite signs [Fig. 1(b)], a localized JR-type state emerges in the band gap. The occurrence of this state has been discussed in previous analytical [34] and experimental [33] studies.

Building upon our discussion in the periodic linear array, we introduce nonlinearities into our model to design a self-induced Dirac mass boundary. Since JR-type modes form at the domain walls separating regions with sign-changing Dirac mass, we can engineer a self-induced JR-type mode by adding to Eq. (1) cubic nonlinearities (described in Supplemental Material, Sec. III [44]) that closely resemble the Kerr nonlinearities found in optics. Specifically, we swap the coefficient of the last term $-(-1)^n\Delta$ with

$$\begin{aligned}2\pi\times f_n(a_n)&=2\pi[f_n^{(0)}-(-1)^n\times\mathrm{sgn}(\delta)\times\beta a_n^2]\\&=2\pi\{f_0+(-1)^n[\delta-\mathrm{sgn}(\delta)\times\beta a_n^2]\},\end{aligned} \quad (3)$$

where f_n is the effective resonance frequency for the nth nonlinear resonator, $\beta>0$ is the third-order nonlinear coefficient, $f_n^{(0)}\equiv f_0+(-1)^n\delta$ are the staggered initial resonance frequencies from the center frequency f_0 and $\mathrm{sgn}(\cdot)$ is the sign function. In this way, the local Dirac mass is $2\pi[\delta-\mathrm{sgn}(\delta)\times\beta a_n^2]$ and the stiffening and softening nonlinearities are represented by the positive and negative signs before the nonlinear coefficient β, respectively.

While the nonlinear detuning of a JR mode in purely stiffening and softening photonic metamaterial was already discussed in a previous numerical study [34], our experimental effort focuses on inducing a sign flip of the Dirac mass using nonlinear effects and thereby creating a self-induced in-gap JR-type state.

To induce this mode in a nonlinear resonator array, we tune the initial resonance frequencies into a staggered configuration and impart upon them alternating types of nonlinearities just as described in Eq. (3). An excitation is then applied on the left edge of the array [Fig. 1(c)] to induce—at high excitation amplitudes—an interface

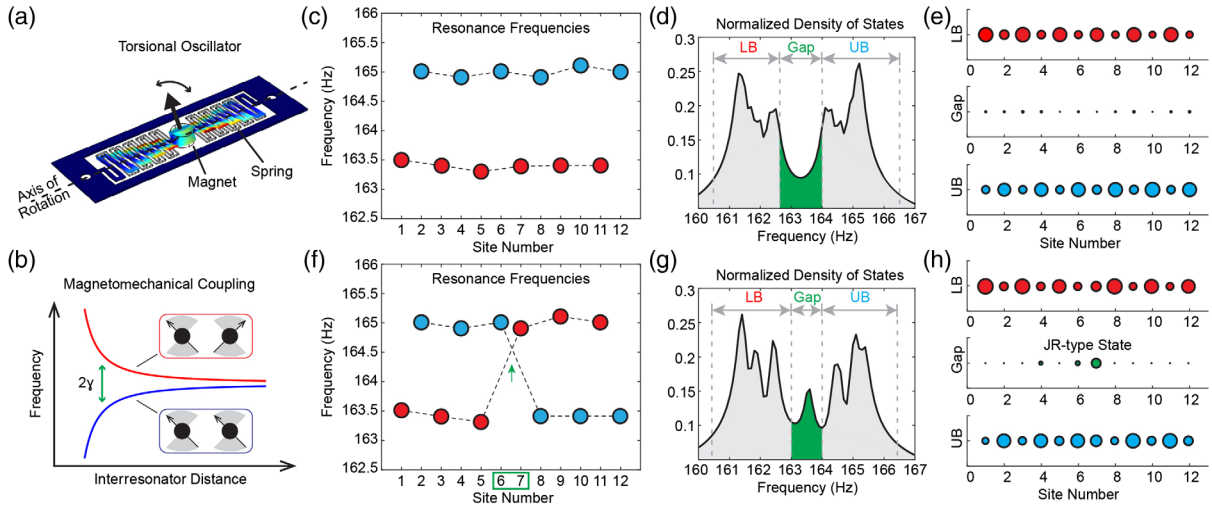

FIG. 2. Experimental realization of Dirac edge mode in a linear magnetomechanical resonator array. (a) In all experiments we utilize single degree-of-freedom magnetomechanical resonators, each having a torsional mechanical mode as illustrated. Color represents total displacement amplitude. (b) The frequency separation between the in-phase (blue line) and the out-of-phase (red line) modes of two adjacent resonators yields the magnetic coupling rate γ. The coupling rate is cubically dependent on distance. The insets depict the hybridized mode shapes for a pair of resonators. Measured γ and geometry details are provided in Supplemental Material, Sec. II [44]. (c) and (f) Individual resonance frequencies for an array without and with the frequency-inversion interface. (d) and (g) The resulting DOS shows an empty or occupied band gap (green) between the upper bulk band (UB) and lower bulk band (LB) colored in gray. (e) and (h) Spatial distributions of the modes are shown in the DOS.

separating the resonators into two regions with positive and negative Dirac masses through designed nonlinear effects. Specifically, we put softening nonlinearity onto resonators with a positive initial frequency offset δ and stiffening nonlinearity onto those with a negative offset $-\delta$. In this way, the Dirac mass $2\pi[\delta - \mathrm{sgn}(\delta) \times \beta a_n^2]$ across this finite chain is linked to the local excitation amplitude a_n. In our experiment, the nonlinear array starts with a uniform negative Dirac mass and a clear band gap. At low levels of excitation, even though nonlinearities on resonators near the edge are weakly evoked, no sign change of the Dirac mass is induced, and thus no in-gap mode was observed [Fig. 1(d)]. When the excitation amplitude reaches a certain threshold, the effective resonance frequencies of the resonator pair closest to the array edge become highly detuned and equalize—closing the local band gap. Further increase of the excitation amplitude flips the effective resonance frequencies and changes the sign of the Dirac mass for this segment, creating an interface within our nonlinear array. Based on our previous argument, a JR-type state at an in-gap frequency would emerge at the interface [Fig. 1(e)]. Increasing the excitation level further recruits more resonator pairs to the side with positive Dirac mass and sends the interface deeper into the gapped array [Fig. 1(f)].

Experimental realization of this model requires a resonator with tunable frequency as well as stiffening or softening nonlinearities. We implement this using magnetomechanical torsional resonators [39] shown in Fig. 2(a). Each resonator is comprised of a disc magnet mounted on a mechanical torsional spring which provides a restoring torque when the resonator is displaced from its neutral angular position. The torsional mode frequency for an isolated resonator is set by the spring stiffness as well as the rotational moment of inertia. We can therefore fine-tune the resonance frequency by mass loading the resonator. The magnetically induced mutual torque between adjacent resonators introduces a coupling that can be condensed into a rate parameter γ [Fig. 2(b)]. In the point-dipole limit, the strength of the magnetomechanical coupling γ decays cubically with increasing distance between the resonators [47,48] allowing us to consider only the nearest-neighbor coupling. Additional details on the magnetomechanical coupling strength γ and photos of our physical setup are provided in Supplemental Material, Secs. II and III [44], respectively.

To study the emergence of the JR-type mode, we first assemble a linear array by placing twelve frequency-tuned resonators into two configurations. For the first configuration, the resonators of high and low resonance frequencies are arranged so that the Dirac mass for the entire array is negative [Fig. 2(c)]. Specifically, resonators on sublattice A and sublattice B have their resonance frequencies tuned to $f_A = 163.5$ Hz and $f_B = 165.0$ Hz, respectively. We keep all resonators at the same height with their torsional axis parallel to one another and set the distance between the centers of the magnets to 2.7 cm for uniform coupling strength. We then measured the mechanical susceptibility of the entire array to probe its density of states (DOS). We locally excite each resonator along the chain via magnetic torque applied using a coil. The resulting angular

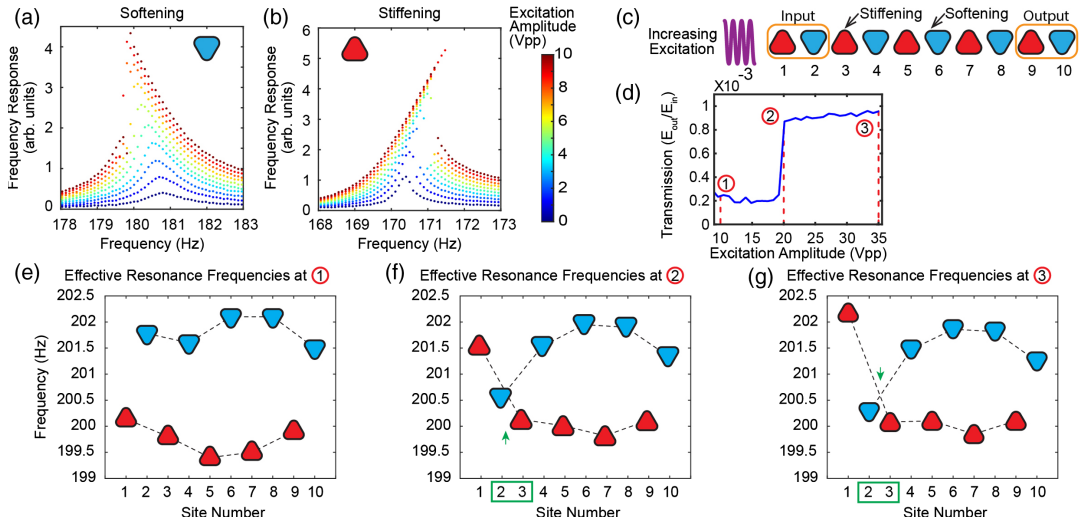

FIG. 3. Realization of a self-induced Dirac boundary mode in a nonlinear array. (a) and (b) Sample frequency response curves for a resonator with spring softening (stiffening) nonlinearity. Note that a different coil system is used in the nonlinear experiment, refer to Supplemental Material, Sec. III [44], Fig. S8 for calibrated nonlinear detuning curves. (c) Configuration for a nonlinear array where energy transmission is defined as output energy over the input (orange boxes). (d) Energy transmission curve as a function of excitation level. (e)–(g) Effective individual resonance frequencies for the nonlinear array at three different excitation levels labeled in the transmission curve.

displacement is then recorded as a function of time through a Hall sensor placed directly below the resonator. To obtain the DOS, frequency scans across the relevant frequency range are performed for each resonator across the chain and the steady-state responses are recorded in increments of 0.1 Hz. The DOS of an array with only the negative Dirac mass is then shown in Fig. 2(d) where a clear band gap is observed. We are also able to plot the excitation pattern for the bulk bands as shown in Fig. 2(e). As expected for a dimerized array, the two bulk modes are separated by a band gap. For the second configuration, we manually flip the resonance frequencies for half of the chain. At the center of this new chain, the Dirac mass changes from negative to a positive value and we expect to see a JR-type mode localized at this interface [Fig. 2(f)]. Indeed, we are able to identify a clear in-gap state from the DOS plot for the second linear chain [Fig. 2(g)]. At the same time, the spatial distribution of the mode, as shown in Fig. 2(h), verifies that this JR-type mode is localized at the interface. Through the comparison between these two different configurations of the linear array, we confirm the correspondence between an inversion of the effective resonance frequencies for resonators on sublattices A and B and the emergence of a localized JR-type state—a conclusion we will use in the nonlinear experiment next.

In order to introduce nonlinearities into the resonator chain as required by Eq. (3), we follow the approach described in a previous study on magnetostatic spring stiffening and softening effects [39]. Specifically, the nonlinearities can be introduced by placing a fixed neodymium magnet near each resonator to generate a local nonuniform ambient magnetic field. In the point-dipole limit, the magnetomechanical resonator experiences a magnetostatic spring effect in addition to the mechanical restoring force. Depending on the relative location and orientation of the magnetic moments, as shown in Supplemental Material, Sec. III [44], the magnetostatic spring effect can produce either softening or stiffening effect with increasing oscillation amplitude. In Figs. 3(a) and 3(b), we show the frequency response of nonlinear softening and stiffening resonators as a function of excitation amplitude. The experimentally measured frequency shifts follow the third-order nonlinearities described in Eq. (3). Additionally, we recorded the effective resonance frequencies at different oscillation amplitudes for every resonator used in the nonlinear resonator chain shown in Supplemental Material, Sec. III [44]. We later use these amplitude-frequency curves to infer the effective resonance frequencies in the nonlinear experiment.

We next construct an array of resonators with alternating types of nonlinearities [see Fig. 3(c)] where a JR-type mode can be induced by strong excitations. The softening resonators are placed on the B sublattice and are tuned to have initial frequencies of around $f_B^{(0)} = 202.0$ Hz. The stiffening resonators on A are tuned to $f_A^{(0)} = 200.0$ Hz. Ten nonlinear resonators spaced 2.7 cm apart are used to build the array. We magnetically excite the array edge at the midgap frequency of $f_{\text{drive}} = 200.8$ Hz by applying a sinusoidal current through a coil placed near the leftmost resonator [Fig. 3(c)]. The excitation voltage applied on the drive coil is linearly proportional to the coil current and the drive torque on the first resonator. At each excitation level, we simultaneously record the steady-state oscillation

amplitudes for all resonators and infer their effective resonance frequencies using the prerecorded amplitude-frequency relation.

To study the energy transmission through the array, we further define a transmission coefficient T:

$$T \equiv \frac{E_{\text{out}}}{E_{\text{in}}} = \frac{a_9^2 + a_{10}^2}{a_1^2 + a_2^2}, \tag{4}$$

where a_n represents the magnitude of oscillation for the nth resonator and $E_{\text{in}}(E_{\text{out}})$ is the input (output) energy defined by the sum of the squares of the oscillation amplitudes for the first (last) unit cell. The energy transmission shows a sudden jump around an excitation level of 20 peak-to-peak voltage (Vpp). As we show next, this jump corresponds to the sudden increase in tunneling via the JR-type mode which acts similarly to an in-gap dopant site in an insulator.

We can confirm the appearance of the JR-type mode by examining the inferred resonance frequencies of the nonlinear chain at a few points of interest [Fig. 3(d)]. For low excitation amplitude, as in Fig. 3(e) for 10 Vpp, the nonlinearities are only weakly invoked and the effective resonance frequencies on A and B sites do not cross, making the Dirac mass negative throughout the chain. For 20 Vpp, we see the first crossing of the resonance frequencies between A and B sites [Fig. 3(f)]. From our previous configuration in Fig. 2, we deduce that a JR-type mode should have appeared in the band gap near the left edge of this nonlinear chain, which in turn facilitated the increased transmission. As the excitation amplitude further increases to 35 Vpp, we observe more frequency tuning but the location of the frequency crossing or the JR-type mode does not change significantly [Fig. 3(g)] and thus T remains stable. In principle, the mode should migrate deeper into the chain and become more localized with even higher excitation as more sites are recruited into the flipped configuration and the crossing of the resonance frequencies between A and B sites becomes steeper (Sec. IV of Supplemental Material [44] discusses mode length scale). Within our experiment range, we observe a digitization behavior in the transmission where T remains at a low "zero state" until the excitation amplitude exceeds the threshold of 20 Vpp where T suddenly jumps up to (and maintains at) a higher level resembling a "one state." Here, the term "digitization" is used to emphasize the binary behavior of the transmission before and after the emergence of an in-gap Dirac boundary state which offers an example of the application for the nonlinear JR-type Dirac boundary mode.

The ability to control both the magnitude and the sign of the excitation mass in Dirac materials has been sought after for its potential to engineer boundary states [15,29]. In this Letter, we demonstrate a resonator array where local nonlinearities can be laid out in a way such that a sign-changing Dirac mass boundary emerges at sufficiently strong drive amplitude and a JR-type boundary mode appears. We further show a novel correspondence between the emergence of a JR-type mode and a sudden improvement of in-gap energy transmission, which is generalizable to all systems with Duffing-type amplitude-frequency nonlinearities. Such nonlinearities are routinely encountered, for example, in macroscale and microscale mechanical devices [49] and in microscale and nanoscale photonic systems [50]. We expect that similar self-induced Dirac boundary states could be realized in higher dimensions where their robustness to disorder along the Dirac mass boundary and tunable dispersion [36] can be used to dynamically modify material properties.

We acknowledge funding support from the U.S. National Science Foundation (NSF) Emerging Frontiers in Research and Innovation program (EFRI) and Office of Naval Research (ONR) Director of Research Early Career Grant (Grant No. N00014-17-1-2209). The authors additionally thank Dr. Inbar Grinberg, Professor Taylor Hughes, and Dr. Xiao-Qi Sun for their valuable insights and discussions.

*bahl@illinois.edu

[1] S.-Q. Shen, *Topological Insulators: Dirac Equation in Condensed Matters* (Springer, New York, 2012), 10.1007/978-3-642-32858-9_2.
[2] Y. Lumer, Y. Plotnik, M. C. Rechtsman, and M. Segev, Phys. Rev. Lett. **111**, 243905 (2013).
[3] T. Kariyado and Y. Hatsugai, Sci. Rep. **5**, 18107 (2016).
[4] V. E. Calado, S. Goswami, G. Nanda, M. Diez, A. R. Akhmerov, K. Watanabe, T. Taniguchi, T. M. Klapwijk, and L. M. K. Vandersypen, Nat. Nanotechnol. **10**, 761 (2015).
[5] J. Fransson, A. M. Black-Schaffer, and A. V. Balatsky, Phys. Rev. B **94**, 075401 (2016).
[6] S. Banerjee, J. Fransson, A. M. Black-Schaffer, H. Ågren, and A. V. Balatsky, Phys. Rev. B **93**, 134502 (2016).
[7] M. Dubois, C. Shi, X. Zhu, Y. Wang, and X. Zhang, Nat. Commun. **8**, 14871 (2017).
[8] R. Chaunsali, E. Kim, A. Thakkar, P. G. Kevrekidis, and J. Yang, Phys. Rev. Lett. **119**, 024301 (2017).
[9] Y. F. Li, F. Meng, S. Li, B. Jia, S. Zhou, and X. Huang, Phys. Lett. A **382**, 679 (2018).
[10] H.-X. Wang, G.-Y. Guo, and J.-H. Jiang, New J. Phys. **21**, 093029 (2019).
[11] Z.-Q. Jiao, S. Longhi, X.-W. Wang, J. Gao, W.-H. Zhou, Y. Wang, Y.-X. Fu, L. Wang, R.-J. Ren, L.-F. Qiao, and X.-M. Jin, Phys. Rev. Lett. **127**, 147401 (2021).
[12] R. Chaunsali, H. Xu, J. Yang, P. G. Kevrekidis, and G. Theocharis, Phys. Rev. B **103**, 024106 (2021).
[13] A. H. Castro Neto, F. Guinea, N. M. R. Peres, K. S. Novoselov, and A. K. Geim, Rev. Mod. Phys. **81**, 109 (2009).
[14] T. O. Wehling, A. M. Black-Schaffer, and A. V. Balatsky, Adv. Phys. **63**, 1 (2014).
[15] G. Giovannetti, P. A. Khomyakov, G. Brocks, P. J. Kelly, and J. van den Brink, Phys. Rev. B **76**, 073103 (2007).

[16] B. Hunt, J. D. Sanchez-Yamagishi, A. F. Young, M. Yankowitz, B. J. LeRoy, K. Watanabe, T. Taniguchi, P. Moon, M. Koshino, P. Jarillo-Herrero, and R. C. Ashoori, Science **340**, 1427 (2013).
[17] L. A. Ponomarenko, R. V. Gorbachev, G. L. Yu, D. C. Elias, R. Jalil, A. A. Patel, A. Mishchenko, A. S. Mayorov, C. R. Woods, J. R. Wallbank, M. Mucha-Kruczynski, B. A. Piot, M. Potemski, I. V. Grigorieva, K. S. Novoselov, F. Guinea, V. I. Fal'ko, and A. K. Geim, Nature (London) **497**, 594 (2013).
[18] B. A. Bernevig, T. L. Hughes, and S.-C. Zhang, Science **314**, 1757 (2006).
[19] M. König, S. Wiedmann, C. Brüne, A. Roth, H. Buhmann, L. W. Molenkamp, X.-L. Qi, and S.-C. Zhang, Science **318**, 766 (2007).
[20] H. Zhang, C.-X. Liu, X.-L. Qi, X. Dai, Z. Fang, and S.-C. Zhang, Nat. Phys. **5**, 438 (2009).
[21] I. Knez, C. T. Rettner, S.-H. Yang, S. S. P. Parkin, L. Du, R.-R. Du, and G. Sullivan, Phys. Rev. Lett. **112**, 026602 (2014).
[22] R. K. Pal and M. Ruzzene, New J. Phys. **19**, 025001 (2017).
[23] G. D'Aguanno, Y. Hadad, D. A. Smirnova, X. Ni, A. B. Khanikaev, and A. Alù, Phys. Rev. B **100**, 214310 (2019).
[24] Z.-G. Chen, L. Wang, G. Zhang, and G. Ma, Phys. Rev. Applied **14**, 024023 (2020).
[25] F. Dreisow, M. Heinrich, R. Keil, A. Tünnermann, S. Nolte, S. Longhi, and A. Szameit, Phys. Rev. Lett. **105**, 143902 (2010).
[26] A. A. Gorlach, D. V. Zhirihin, A. P. Slobozhanyuk, A. B. Khanikaev, and M. A. Gorlach, Phys. Rev. B **99**, 205122 (2019).
[27] M. Xiao, Z. Q. Zhang, and C. T. Chan, Phys. Rev. X **4**, 021017 (2014).
[28] R. Jackiw and C. Rebbi, Phys. Rev. D **13**, 3398 (1976).
[29] G. W. Semenoff, V. Semenoff, and F. Zhou, Phys. Rev. Lett. **101**, 087204 (2008).
[30] W. Yao, S. A. Yang, and Q. Niu, Phys. Rev. Lett. **102**, 096801 (2009).
[31] S. Longhi, Opt. Lett. **35**, 235 (2010).
[32] D. G. Angelakis, P. Das, and C. Noh, Sci. Rep. **4**, 6110 (2014).
[33] W. Tan, Y. Sun, H. Chen, and S.-Q. Shen, Sci. Rep. **4**, 3842 (2014).
[34] T. X. Tran and F. Biancalana, Phys. Rev. A **96**, 013831 (2017).
[35] Y. Sharabi, Y. Plotnik, Y. Nemirovsky, and M. Segev, in *Proceedings of the 2018 Conference on Lasers and Electro-Optics (CLEO)* (Optica Publishing Group, Washington, DC, 2018), pp. 1–2, 10.1364/CLEO_QELS.2018.FM1E.3.
[36] O. Shtanko and L. Levitov, Proc. Natl. Acad. Sci. U.S.A. **115**, 5908 (2018).
[37] E. Y. Ma *et al.*, Nat. Commun. **6**, 7252 (2015).
[38] F. Nichele, H. J. Suominen, M. Kjaergaard, C. M. Marcus, E. Sajadi, J. A. Folk, F. Qu, A. J. A. Beukman, F. K. d. Vries, J. v. Veen, S. Nadj-Perge, L. P. Kouwenhoven, B.-M. Nguyen, A. A. Kiselev, W. Yi, M. Sokolich, M. J. Manfra, E. M. Spanton, and K. A. Moler, New J. Phys. **18**, 083005 (2016).
[39] I. H. Grinberg, A. Mangu, C. W. Peterson, E. Wilken-Resman, J. T. Bernhard, and G. Bahl, IEEE Trans. Magn. **55**, 1 (2019).
[40] E. B. Herbold, J. Kim, V. F. Nesterenko, S. Y. Wang, and C. Daraio, Acta Mech. **205**, 85 (2009).
[41] A. A. Maradudin, P. Mazur, E. W. Montroll, and G. H. Weiss, Rev. Mod. Phys. **30**, 175 (1958).
[42] J. Ruseckas, V. Kudriašov, G. Juzeliūnas, R. G. Unanyan, J. Otterbach, and M. Fleischhauer, Phys. Rev. A **83**, 063811 (2011).
[43] T. X. Tran, S. Longhi, and F. Biancalana, Ann. Phys. (Amsterdam) **340**, 179 (2014).
[44] See Supplemental Material at http://link.aps.org/supplemental/10.1103/PhysRevLett.129.135501 for details on (i) equations of motion and their link to the 1D Dirac equation, (ii) magnetomechanical coupling strength, (iii) resonator nonlinearity control, and (iv) boundary state length scale.
[45] P. A. M. Dirac and R. H. Fowler, Proc. R. Soc. A **117**, 610 (1928).
[46] C. D. Anderson, Phys. Rev. **43**, 491 (1933).
[47] I. H. Grinberg, M. Lin, C. Harris, W. A. Benalcazar, C. W. Peterson, T. L. Hughes, and G. Bahl, Nat. Commun. **11**, 974 (2020).
[48] I. H. Grinberg, M. Lin, W. A. Benalcazar, T. L. Hughes, and G. Bahl, Phys. Rev. Applied **14**, 064042 (2020).
[49] T. Roessig, R. Howe, and A. Pisano, in *Proceedings of the IEEE International Frequency Control Symposium* (IEEE, Orlando, 1997), pp. 778–782, 10.1109/FREQ.1997.639190.
[50] H. S. Eisenberg, Y. Silberberg, R. Morandotti, A. R. Boyd, and J. S. Aitchison, Phys. Rev. Lett. **81**, 3383 (1998).